Photoabsorption spectra of the heavy alkali-metal negative ions

Chris H. Greene
Department of Physics and Joint Institute for Laboratory Astrophysics, University of Colorado, Boulder, Colorado 80309-0440
(Received 12 April 1990)

The combined use of an eigenchannel R-matrix calculation in jj coupling, and of a generalized quantum-defect treatment of electron escape in a polarization potential, accounts quantitatively for high-resolution photodetachement spectra of Cs^- and Rb^-. The calculation further predicts the existence of three odd-parity $6s6p\ ^3P^o$ bound states in Cs^- (with $J=0,1,2$) in addition to the well-known $6s^2$ ground state, confirming earlier evidence derived from studies by Fabrikant [Opt. Spektrosk. **53**, 223 (1982); Eng. trans., Opt. Spectrosc. (USSR) **53**, 131 (1982)], and by Fischer and Chen [J. Mol. Struc. **199**, 61 (1989)] performed in LS coupling. The radiative lifetime of the $J=1$ excited bound state is predicted to be 0.013 sec, whereas the $J=0,2$ fine-structure components appear to be unusually long-lived. Photodetachment spectra predicted for Fr^- exhibit resonances near the first excited ^2P thresholds of Fr, analogous to those familiar in Rb^- and Cs^-.

I. INTRODUCTION

Prominent narrow resonance features observed[1-4] in the alkali-metal negative ions near the first excited np thresholds have proved difficult to describe quantitatively. Lee's multichannel effective range model[5] neglected the long-range interaction between the Cs atom and the escaping photoelectron. As Patterson *et al.*[2] pointed out, this approximation is highly doubtful since the polarizability of Cs($6p$) is greater than $10^3 a_0^3$. Nevertheless, by fitting his nine-parameter model to the experimental total photodetachment spectrum, Lee obtained a reasonably good description of the resonance profiles. He also used the fitted parameters to predict a number of other observables, notably partial detachment cross sections which were found to agree well with subsequent measurements.

Quantitative calculations by Taylor and Norcross[6] for the simpler but similar system K^- showed that the meromorphic (rescaled) reaction matrix varies *substantially* with energy even over the small spin-orbit splitting ≈ 58 cm^{-1} of K($4p$). Lee's assumption that this matrix is independent of energy over 550 cm^{-1} in Cs^- was clearly shown to be incorrect, although the model still apparently has some utility for phenomenological interpretation. Watanabe and Greene[7] (cited as WG below) showed meanwhile that the strong energy dependence of the reaction matrix calculated by Taylor and Norcross for K^- derived solely from the long-range polarization potential of the K($4p$) state, and could be handled analytically in terms of the known closed-form (Mathieu) solutions to the Schrödinger equation in this long-range potential. The WG treatment amounts to a generalization of Seaton's multichannel quantum-defect theory[8] (MQDT) to describe electron motion in the long-range potential $-\alpha/2r^4$ instead of in an attractive Coulomb potential. This generalized MQDT formulation has been used to describe negative-ion properties in a number of different contexts.[9]

Small-scale eigenchannel R-matrix calculations, conducted in LS coupling in recent years for all the alkaline-earth atoms,[10-13] show that excellent agreement with experimental spectra can be achieved at a modest computational expense. The first key to making such calculations work for heavy atoms (especially Ca, Sr, Ba, Ra) is the incorporation of experimental information to determine an effective one electron potential $V(r)$ which is *constrained* to give accurate energy levels of the one-electron system.[14] This empirical constraint on the one-electron properties seems to be all that is required to guarantee the accuracy of calculated *two-electron* spectra. It is also crucial to include effects of the spin-orbit interaction, in order to interpret high resolution photoabsorption spectra of the type presently available.[15] The comparatively weak spin-orbit interaction generates conspicuous effects even in light atoms, because Rydberg series converging to fine-structure-split ionization thresholds interfere and perturb each other strongly. In the calculations of Refs. 10, 12, and 13, a simple angular momentum recoupling suffices to convert the LS-coupled reaction matrices of multichannel quantum-defect theory into a jj-coupled reaction matrix.[8] This frame transformation procedure has been shown in numerous studies to describe alkaline-earth atomic dynamics with an accuracy comparable to, and in many respects better than, that of experimental capabilities.

For heavier atoms such as Ba and Ra this frame transformation method for describing fine-structure effects becomes less valid because the de Broglie phase of an electron is increasingly dependent on the value of $j=s+l$. This j dependence of the phase is accounted for in the frame transformation approach only at comparatively large electron distances from the nucleus. Difficulties with the frame transformation procedure are further amplified in the alkali-metal negative ions because the binding of the outermost electron to the one-electron residue is far weaker than in neutral atoms.

The main goal of this study is the development of the capability to include the strong spin-orbit effects present in heavy alkali-metal negative ions, but without relying

on the approximations inherent in the *jj-LS* frame transformation. The combination of this technology with an MQDT description of electron motion in strong polarization potentials is shown to give an excellent description of photodetachment resonances observed for Rb^- and Cs^-. When the full R-matrix calculation is set up in *jj* coupling to better describe spin-orbit effects, the number of *jj*-coupled channels is substantially larger (typically a factor of 3 larger) than the corresponding *LS*-coupled calculations. Nevertheless, the computations are still small enough to carry out efficiently on a small computer workstation. The success of the calculations permits a deeper investigation of assumptions made in previous semiempirical MQDT analyses of the spectra, showing for instance that Lee's neglect[5] of d waves is partly responsible for deficiencies in his empirical fit to the observed Cs^- spectrum.[1,2]

Predictions are also made concerning the excited odd-parity bound levels of Cs^-. These have not been directly observed in any experiment, but there is growing theoretical evidence for their existence.[16–19] Finally the photodetachment spectrum of Fr^- is predicted, which may permit a critical test of calculations ignoring relativistic effects beyond the spin-orbit interaction, when the spectrum is eventually observed.

II. SPECIFIC ASPECTS OF THE CALCULATIONS

The following describes an implementation of the eigenchannel R-matrix formulation[10–13] using a nonperturbative treatment of spin-orbit effects which goes beyond the simple *jj-LS* frame transformation. The main new element is the inclusion of the spin-orbit interaction V_{so} term for each electron in addition to the potential energy $V(r)$, having the form (in a.u.)

$$V_{so}=\frac{\mathbf{s}\cdot\mathbf{l}}{2c^2}\frac{1}{r}\frac{\partial V}{\partial r}\left[1-\frac{V(r)}{2c^2}\right]^{-2}. \tag{1}$$

Here $c=137.036$ is the speed of light in atomic units. The last factor in Eq. (1) is suggested by the Dirac equation and has been used elsewhere.[20] It renormalizes the singularity of the spin-orbit term and makes solutions to the radial Schrödinger equation well behaved at the nucleus. It should be noted that the Wigner-Eisenbud R-matrix calculations of Refs. 14 and 19 also include spin-orbit effects at the level of Eq. (1).

The one-electron potential $V(r)$ is chosen conveniently to have the following analytical form, following Aymar:[21]

$$V(r)=\frac{1}{r}[Z_c+(Z-Z_c)e^{-a_1 r}+a_2 r e^{-a_3 r}]-\frac{\alpha_c}{2r^4}(1-e^{-(r/r_c)^6}). \tag{2}$$

The nuclear charge is $Z=55$ for the Cs^- calculation, while the charge of the rare-gas-like core is $Z_c=1$. The polarizability of the rare-gas ion Cs^+ is taken to be $\alpha_c=15.644$ a.u. from Ref. 22. (The values of α_c for the rare-gas-like ion Rb^+ is taken as 9.076 a.u. from Ref. 23, while that of Fr^+ has been crudely estimated as 22 a.u.) Finally the four empirical parameters (a_1,a_2,a_3,r_c) are simply adjusted in a least-squares fitting program until the energy eigenvalues of the one-electron Schrödinger equation reproduce the experimental spectrum, i.e., the spectrum of Cs in the present calculation. To get optimum agreement with the experimental one-electron levels, it is preferable to allow the parameters to be l dependent, at least for atoms heavier than argon. The resulting one-electron potential is then local in r but nonlocal in each electron's angular coordinates, but this nonlocality is trival in origin and causes no further complications in the calculation. It is to be emphasized that experience in conducting numerous R-matrix calculations in Refs. 10–13 has shown that the final two-electron spectra are highly *insensitive* to the actual one-electron potential used, as long as the resulting one-electron energy levels are accurate.

The rest of the calculation proceeds along the same lines as the R-matrix calculations performed previously in *LS* coupling, with some obvious modifications. That is, a two-electron variational basis is constructed using the one-electron radial eigenfunctions $u_{nlj}(r)$ calculated within the finite R-matrix reaction volume ($r<r_0$), using the potential $V(r)+V_{so}(r)$. These eigenfunctions have the *jj*-coupled structure

$$y_k=\mathcal{A}\,u_{n_1 l_1 j_1}(r_1)u_{n_2 l_2 j_2}(r_2)\{[\chi^{(1/2)}(1)\otimes Y^{(l_1)}(1)]^{(j_1)}\otimes[\chi^{(1/2)}(2)\otimes Y^{(l_2)}(2)]^{(j_2)}\}^{(J)}, \tag{3}$$

where $\mathcal{A}$ is an antisymmetrization operator, χ represents an electron spinor, and $Y^{(l)}$ denotes a spherical harmonic. Matrix elements of the electron-electron interaction $1/r_{12}$ and of the dipole length and velocity operators in this *jj*-coupled basis set are obtained using standard Wigner-Racah algebra.

As discussed in Refs. 10 and 13, each one-electron basis orbital $u_{nlj}(r)$ which vanishes on the reaction surface $r=r_0$ is termed a "closed-type" orbital, while those nonzero at r_0 are the "open-type" orbitals. The great majority of the two-electron basis functions (3) consists of two closed-type radial orbitals for $u_{n_1 l_1 j_1}(r_1)$ and $u_{n_2 l_2 j_2}(r_2)$ (typically 200–400 such "closed-type" basis functions). But for every channel to be retained in the final multichannel quantum-defect treatment, a pair of "open-type" two-electron basis functions is included, each consisting of one closed-type orbital and one open-type orbital. In the Cs^- calculation near and below the cesium ground-state energy, two channels are included for $J=1$, odd parity, namely, $6s_{1/2}\epsilon p_{1/2}$ and $6s_{1/2}\epsilon p_{3/2}$. Instead for $J=0$ (or for $J=2$) only the first (second) of these channels is retained in the final MQDT calculation of observables. The photodetachment calculations conducted near the first excited $^2P^o$ thresholds utilize seven

$J=1$ channels, given in Table I.

After the variational R-matrix calculation obtains logarithimic derivatives of the escaping electron's wave function at the reaction surface, these logarithimic derivatives are converted[10–13] into a smooth (i.e., meromorphic), short-range reaction matrix $\underline{\mathbf{K}}^0$. This is found here as in previous calculations, by matching the wave function in the i-th channel to two independent solutions (f_i^0, g_i^0) of the radial Schrödinger equation of an electron in the polarization potential appropriate for that channel. These radial solutions, analytic functions of energy, are expressed in terms of Mathieu functions in WG.[7] The polarization potential was determined by a separate calculation using only closed-type one-electron orbitals u_{nlj} (still confined to the R-matrix box) to represent the residual atomic valence electron, yielding an effective polarizability $\alpha_i \equiv \alpha_{n_1 l_1 j_1 l_2 j_2}$ relevant to each jj-coupled channel. The resulting polarizabilities for all relevant channels are given in Table I. The polarizability for the $Cs^-(6s\epsilon p)$ channels is 10% larger than the value obtained in the more accurate calculation of Zhou and Norcross,[22] while the values for the $6p\epsilon s$ channels agree with Ref. 22 at about the 5% level. The expression for channel polarizabilities is derived from an adiabatic diagonalization of the close-coupling equations at large radii, along the same lines as those presented in Appendix A of WG, giving for the present situation in which the channels are jj coupled instead of LS coupled,

TABLE I. Effective channel polarizabilities (in a.u.) for jj-coupled channels of Rb^- ($n=5$), Cs^- ($n=6$), and Fr^- ($n=7$).

Channel, i	$\alpha_i(Rb^-)$	$\alpha_i(Cs^-)$	$\alpha_i(Fr^-)$
$ns_{1/2}\epsilon p_{1/2}$	343.3	440.6	341.4
$ns_{1/2}\epsilon p_{3/2}$	343.3	440.6	341.4
$np_{1/2}\epsilon s_{1/2}$	831.3	1394.0	1209.9
$np_{1/2}\epsilon d_{3/2}$	831.3	1394.0	1209.9
$np_{3/2}\epsilon s_{1/2}$	893.6	1669.6	2042.5
$np_{3/2}\epsilon d_{3/2}$	925.2	1718.0	2124.9
$np_{3/2}\epsilon d_{5/2}$	1020.1	1863.3	2372.1

$$\alpha_{n_1 l_1 j_1 l_2 j_2} = 2 \sum_{n_1' l_1' j_1' l_2' j_2'} \frac{|\langle n_1(s_1 l_1) j_1 (s_2 l_2) j_2 JM | r_1 \cos\theta_{12} | n_1'(s_1 l_1') j_1' (s_2 l_2') j_2' JM \rangle|^2}{E_{n_1' l_1' j_1'} - E_{n_1 l_1 j_1}} . \tag{4}$$

Note that the channel polarizability reduces to the usual static polarizability in some cases, such as when either electron has zero orbital angular momentum. Two approximations are thus being made in the description of electron escape beyond the R-matrix box radius. First, effects of the r^{-2} dipole interaction are included *adiabatically* for $r > r_0$, which converts the r^{-2} off-diagonal interaction into an effective long-range potential $-\alpha_i/2r^4$ in the i-th channel, if there are no "accidental" degeneracies. Second, the interaction of the photoelectron with the Cs($6p$) electric quadrupole moment has been neglected, but this interaction vanishes for all channels shown in Table I, except for $6p_{3/2}\epsilon d_{3/2}$ and $6p_{3/2}\epsilon d_{5/2}$. Since these two channels have extremely small partial cross sections in the energy range studied in this paper, neglect of the $6p$ quadrupole moment should be an excellent approximation, though worth reconsidering in other contexts.

To connect with previous eigenchannel quantum defect treatments, it is convenient to express the real, symmetric $\underline{\mathbf{K}}^0$ in terms of its eigenvalues $\tan\pi\mu_\alpha$ and eigenvectors $U_{i\alpha}$. The superscript 0 will be dropped from μ_α and $U_{i\alpha}$ for simplicity, though it should be remembered that they are analytic functions of energy. The corresponding eigenchannels Ψ_α of the reaction matrix have the following form at $r \geq r_0$:

$$\Psi_\alpha = \mathcal{A} r^{-1} \sum_i \Phi_i(\Omega) U_{i\alpha} [f_i^0(r)\cos\pi\mu_\alpha - g_i^0(r)\sin\pi\mu_\alpha] , \tag{5}$$

in which the close-coupling-type channel function $\Phi_i(\Omega)$ coincides with Eq. (3) except that $u_{n_2 l_2 j_2}(r_2)$ is omitted. Note that Ω stands for all spatial and spin coordinates of the electron pair, except for the radial coordinate r of the outermost electron. A reduced dipole matrix element connecting each eigenstate in Eq. (5) to the negative-ion ground-state Ψ_0 is defined in the usual way, e.g., in the velocity gauge

$$D_\alpha = \omega^{-1} \langle \Psi_\alpha \| \nabla_1^{(1)} + \nabla_2^{(1)} \| \Psi_0 \rangle . \tag{6}$$

Some properties of the radial solutions (f_i^0, g_i^0) are crucial for the practical implementation of MQDT for systems having a long-range polarization potential. Most important is the fact that they are analytic functions of energy, because they are energy independent at $r \to 0$. [See Eqs. (2.8) of WG.[7]] Each comparison solution obeys the following radial Schrödinger equation (in a.u.):

$$\left[-\frac{1}{2}\frac{d^2}{dr^2} + \frac{l_i(l_i+1)}{2r^2} - \frac{\alpha_i}{2r^4} - \varepsilon_i \right] f_i^0(r) = 0 , \tag{7}$$

and similarly for $g_i^0(r)$. Being analytic, (f_i^0, g_i^0) exhibit no singularities at photodetachment thresholds, and consequently the short-range MQDT parameters μ_α, $U_{i\alpha}$, and D_α are also analytic functions of energy. It should be stressed that even though the solutions (f_i^0, g_i^0) obey the differential equation (7) at all radii, they are only used here *outside* the reaction surface $r = r_0$ and *not* at small radii where the r^{-4} potential is unrealistic. In effect these solutions provide a method to analytically "propagate" the numerical solution, determined variationally within $r \leq r_0$, outward to $r \to \infty$ where boundary conditions will ultimately be imposed in the course of solving Eq. (9) below.

In the standard close-coupling nomenclature, channel energies of an escaping photoelectron are defined by $\varepsilon_i \equiv E - E_i$, where E is the total final state energy and E_i

is the detachment threshold energy in channel i. Channel i is said to be closed or open depending on whether the channel energy ε_i is negative or positive, respectively. The radial solutions (f_i^0, g_i^0) diverge exponentially at $r \to \infty$ in closed channels; in standard MQDT fashion, the degenerate eigenchannels Ψ_α in Eq. (5) must be superposed (i.e., $\psi = \sum_\alpha \Psi_\alpha a_\alpha$) to eliminate the divergent components. This step requires the asymptotic forms of the radial solutions. These have simpler, standard expressions in terms of a different "energy-normalized" base pair of radial solutions (f_i, g_i), related to (f_i^0, g_i^0) by a Wronskian-preserving linear transformation

$$f_i(r) = A_i^{1/2} f_i^0(r) , \tag{8a}$$

$$g_i(r) = A_i^{-1/2}[\mathcal{G}_i f_i^0(r) + g_i^0(r)] . \tag{8b}$$

[The energy- and channel-dependent parameters $A_i, \mathcal{G}_i$ can be calculated for any long-range potential, and are derived for solutions of Eq. (7) in WG. Note that the parameter A_i was denoted B_i at positive channel energies in WG.] Asymptotic expressions for these energy-normalized solutions are then given by Eqs. (2.12), and (2.13) of WG, in terms of energy- and channel-dependent phase parameters $(\beta_i \eta_i)$ defined in Eqs. (2.17) of WG. [For a repulsive polarizability potential having $\alpha_i < 0$, see instead Watanabe.[9(a)] This case is not encountered for any channel in the present paper, but for instance the $Cs^-(5d\epsilon l)$ channels do have negative values of α_i.]

III. MQDT CALCULATIONS FOR Cs^-, Rb^-, AND Fr^-

The usual equations of generalized MQDT are now used to analytically impose boundary conditions at $r \to \infty$. This results in the following generalized eigenvalue problem to be solved at each value of the final-state energy E:

$$\underline{\Gamma}\mathbf{a} = \tan\pi\tau\,\underline{\Lambda}\mathbf{a} , \tag{9}$$

where

$$\Gamma_{i\alpha} = \begin{cases} U_{i\alpha}\sin(\tilde{\beta}_i + \pi\mu_\alpha), & i \in Q \\ U_{i\alpha} A_i \sin\pi\mu_\alpha, & i \in P \end{cases}$$

$$\Lambda_{i\alpha} = \begin{cases} 0, & i \in Q \\ U_{i\alpha}(\cos\pi\mu_\alpha + \mathcal{G}_i \sin\pi\mu_\alpha), & i \in P . \end{cases} \tag{10}$$

In Eq. (10) Q and P denote sets of the closed and open detachment channels, respectively. The modified phase parameter $\tilde{\beta}$ is defined for closed channels along the lines of Kim and Greene:[9(c)]

$$\tilde{\beta}_i = \arctan[(A_i \cot\beta_i + \mathcal{G}_i)^{-1}] . \tag{11}$$

Each of the parameters β_i, $\mathcal{G}_i$, and A_i are defined in WG, and shown to depend on the energy and polarizability in channel i only through the product form $\varepsilon_i \alpha_i$. These parameters are tabulated in WG for an s-wave photoelectron, and for p waves and d waves see Ref. 24.

The number of nontrivial eigensolutions of Eq. (9) coincides with the number of open channels N_0. An $N_0 \times N_0$ orthogonal matrix $T_{i\rho}$ representing eigenvectors of the physical scattering matrix can be constructed as

$$T_{i\rho} = \sum_\alpha \left[A_i^{-1/2}(\cos\pi\mu_\alpha + \mathcal{G}_i \sin\pi\mu_\alpha)\cos\pi\tau_\rho + A_i^{1/2}\sin\pi\mu_\alpha \sin\pi\tau_\rho \right] a_{\alpha\rho} . \tag{12}$$

The solution vectors $a_{\alpha\rho}$ of the homogeneous system Eq. (9) are normalized such that Eq. (12) is a real, orthogonal matrix, which guarantees that the final "collision eigenchannel" solutions $\psi_\rho = \sum_\alpha \Psi_\alpha a_{\alpha\rho}$ are energy normalized.[7] These results modify the MQDT equations of Ref. 25 [Eqs. (24), (25), and (20a)] to account for the fact that "analytic" reference solutions (f_i^0, g_i^0) are used in defining the reaction matrix $\underline{K}^0$ rather than "energy-normalized" reference solutions. If energy-normalized radial solutions (f_i, g_i) are used in any channel instead of the analytic radial base pair, Eqs. (10–12) are modified by replacing A_i by unity, $\mathcal{G}_i$ by zero, and $\tilde{\beta}_i$ by β_i in that channel. With these generalizations, Eqs. (28)–(32) of Ref. 25 can be used without further modification to determine the total and partial photodetachment cross sections, or to calculate other observables such as the photoelectron angular distribution.

A. Cs^-

Two separate calculations have been performed for $J = 1$, odd-parity states of Cs^-, namely, a two-channel calculation near the Cs(6s) detachment threshold and a seven-channel calculation near the Cs(6p) thresholds. All calculations shown in this paper were obtained using an R-matrix box radius of $r_0 = 30$ a.u. Table II shows the lowest odd-parity energy levels obtained in the MQDT calculations conducted near the ground-state energy of Cs. The presence of three bound levels for Cs^- in Table II is consistent with the classification $^3P^o$ found in the LS-coupled calculation of Fischer and Chen[16] and is also consistent with Fabrikant's[17] extrapolation. The $(2J+1)$-weighted average of the energies in Table II is $E_{av} = 18$ meV, which lies within the spread of $^3P^o$ levels calculated previously in Refs. 16–18.

Normally, calculated two-electron energy levels are somewhat lower than experimental levels when a model

TABLE II. Predicted energies for the Cs^- $^3P^o$ bound levels

$Cs^-(6s6p\,^3P^o)$ level	Electron affinity (meV) Present calculation	Others
$J=0$	32	
$J=1$	25	
$J=2$	11	
Average	18	27[a] between 1 and 11[b] 12[c]

[a]Extrapolation of Fabrikant, Ref. 17.
[b]Fischer and Chen MCHF calculation, Ref. 16.
[c]Krause and Berry, Ref. 18 (this value was discounted as spurious in Ref. 18).

potential is used without including the repulsive "dielectronic polarization term" omitted in the present study. For instance, the binding energy of the outermost electron in the $6s^2\ J^\pi=0^+$ state is calculated to be 0.52 eV, which is 10% deeper than the experimental electron affinity of 0.4715 eV.[2] But this term is mainly important where both electrons are at comparable distances from the core, as in the $6s^2$ state, and far less important for extremely weakly bound levels such as the odd-parity $J=0,1,2$ levels. Nevertheless, the model Hamiltonian used here may overestimate the binding for this reason. But the good results shown below for the photodetachment cross section at higher energies lend indirect support to the conclusion that the $^3P^o$ levels are bound for Cs^-. Further indirect evidence that they are bound can be seen in the eigenphase sums for e-Cs scattering from Fig. 1 of Ref. 19, which show no evidence of a $^3P^o$ shape resonance above the Cs($6s$) threshold. This suggests that it would probably be located below that threshold, making it stable.

Interestingly, the $^3P^o$ level was also found to be stable, by 12 meV, in the calculation of Krause and Berry,[18] but these authors argued that this is a spurious result due to inaccuracies in their calculation. Electron correlation at small distances clearly plays a critical role in causing the $6s6p\ ^3P^o$ level to be bound, but the small binding energy implies that the outermost electron spends most of its time far outside the inner Cs($6s$) electron. Accordingly this state seems better labelled by independent-electron quantum numbers than by collective or rotor-vibrator quantum numbers.

Electric dipole transitions between the Cs^-6s^2 ground state and the $^3P^o_{J=1}$ level are allowed but weak because of the spin selection rule. Length and velocity absorption oscillator strengths obtained for this transition are $f_L=6.9\times10^{-6}$ and $f_V=2.1\times10^{-5}$. The poor agreement between length and velocity is not unusual for such a small value of the oscillator strength. Using f_V, as is usually more reliable in these calculations, the lifetime of the $J=1$ excited bound state is estimated to be quite long: $\tau=0.013$ sec. This long lifetime should be easily adequate for observation in any typical beam experiment, but the small oscillator strength will make the direct photoexcitation of the $6s6p\ ^3P^o$ level from the ground state extremely difficult. A more plausible method to detect this state could be the photodetachment of one of the $^3P^o$ bound components at a laser frequency which reaches the

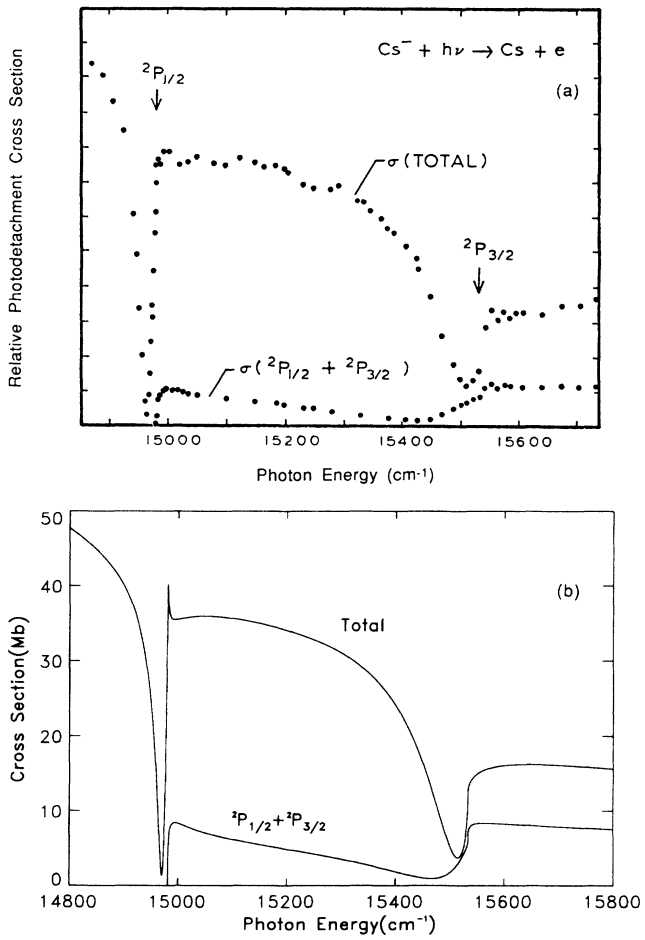

FIG. 1. Total and partial cross sections for Cs^- photodetachment near the $6p_{1/2}$ and $6p_{3/2}$ thresholds. (a) Measured relative cross sections of Slater *et al.*, from Ref. 2 (b) Present calculation.

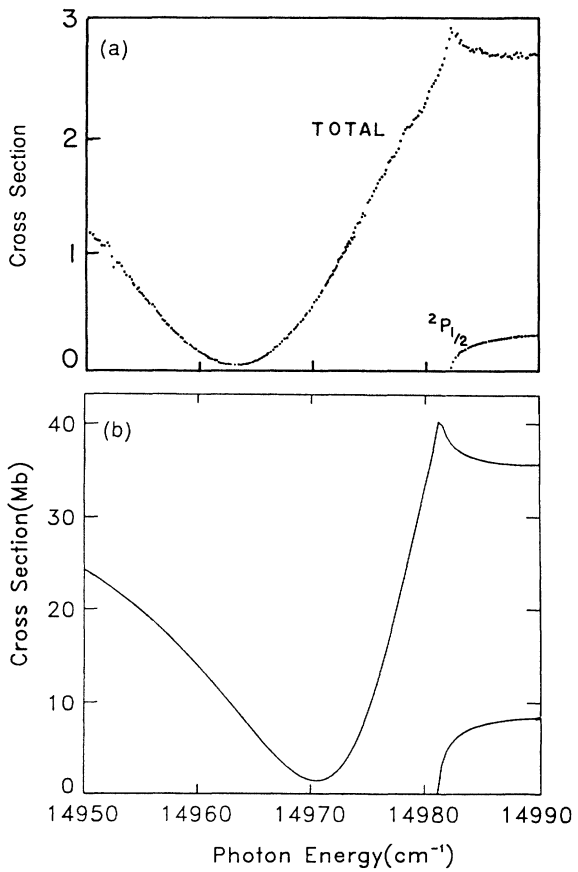

FIG. 2. Expanded view of the cross sections shown in Fig. 1, showing the cusp at the $6p_{1/2}$ threshold and the nonzero minimum below that threshold. (a) Unpublished experimental relative cross sections of Schulz and Lineberger, from Ref. 26. (b) Present calculation.

vicinity of the $6p_{1/2}$ threshold of Cs, where it should be possible to excite the $6p^2$ resonance components.[19] Compared to the $6s6p\ ^3P^o_{J=1}$ level, the radiative lifetimes of the $J=0$ and $2\ ^3P^o$ levels should be orders of magnitude longer, because they involve emission of three electric-dipole photons (in the absence of hyperfine interactions) in addition to being spin forbidden.

It is worth noting that an application of the simpler *jj-LS* frame transformation in the energy range close to the $Cs(6s_{1/2})$ threshold would give results identical to a purely *LS*-coupled calculation since this threshold has no fine-structure splitting. Consequently the *jj-LS* frame transformation would make two incorrect predictions: first that the $6s6p\ ^3P^o$ bound level would have no spin-orbit splitting, and second that the oscillator strength connecting the $J=1$ level to the Cs^- ground state should vanish.

Figure 1 compares the experimental cross section measured by Slater *et al.*[2] for photodetachment of the $6s^2$ ground state in the vicinity of the excited $Cs(6p)$ thresholds, with the present seven-channel calculation. (As in Refs. 12 and 13, the experimental ground state energy of Cs^- has been used in relating the photon energy to the final state energy, in Figs. 1–4 of this paper.) The striking resonance features near each threshold, which might be labelled as $6p_j7s$ Feshbach resonances, are well reproduced, except for some minor differences. A pronounced cusp in the calculated total cross section right at the $6p_{1/2}$ threshold is possibly visible in the experimental cross section, but it is substantially smeared out by the finite experimental resolution. In the present study, the length and velocity forms for the cross section typically agree to better than 10%; only the velocity results are shown here.

Figure 2 compares the calculation on an expanded scale near the cusp at the $6p_{1/2}$ threshold to unpublished photodetachment measurements obtained at higher resolution by Schulz *et al.*[26] In this measurement the cusp is clearly visible, rising approximately 10% higher than the flat region of the total cross section at 14 990 cm^{-1}, compared to the calculated cusp height of 14%. The presence or absence of a threshold cusp is difficult to predict in advance, as it depends sensitively on the specific values of the short-range MQDT parameters. Another feature of the measured spectrum clearly visible in Fig. 2(a) is the nonzero minimum near 14 963 cm^{-1}, where the total cross section is roughly 2% of the flat cross-section value. All attempts to fit Lee's multichannel effective range model to this spectrum result in an exact zero of the cross section in this energy range, because Lee neglects the dipole matrix elements connecting the $6s^2$ ground state to the $^3P^o$ final state eigenchannels. On the other hand the present calculation including fine-structure effects in the reaction zone produces eigenchannels that are not strictly *LS* coupled, agreeing qualitatively with experiment in having a nonzero minimum. The depth of the calculated minimum is close to 4% of the flat background, and its position is shifted 8 cm^{-1} higher than the experimental minimum.

The partial cross section for production of excited Cs atoms in Fig. 1 is also in generally good agreement with experiment, except for its shape just below the $6p_{3/2}$ threshold. It is somewhat surprising that the shapes of the experimental and calculated resonances below the

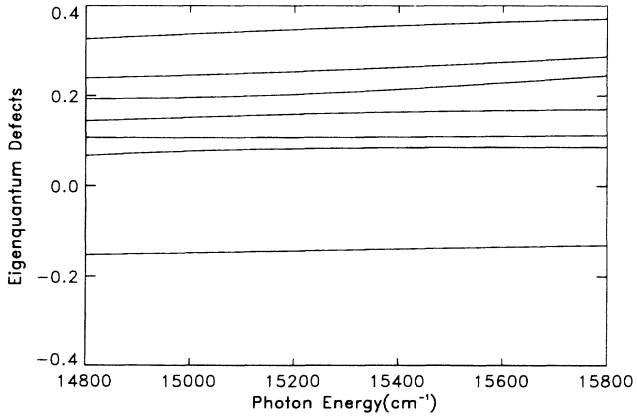

FIG. 3. Calculated eigenquantum defects μ_α in the generalized polarizability representation for the MQDT parameters, showing them to be far smoother functions of energy than the calculated photodetachment spectra.

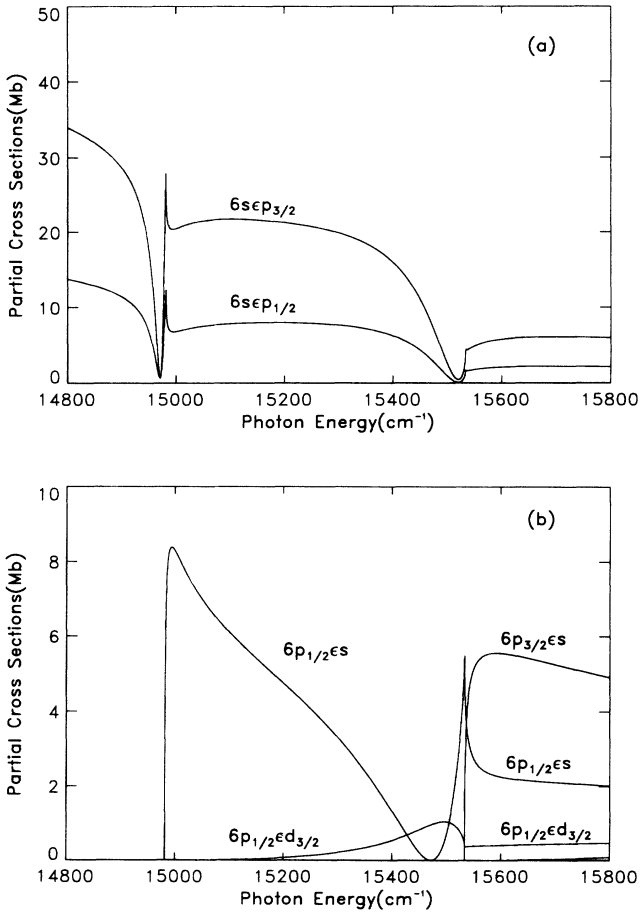

FIG. 4. Partial cross sections predicted by the present calculation of Cs^- photodetachment. (a) Fast photoelectrons leaving behind atomic cesium in its ground state. (b) Slow photoelectrons associated with production of excited cesium atoms.

$6p_{3/2}$ threshold agree much more closely in the total cross section than in the partial cross section. The overall magnitudes of the experimental and theoretical partial cross sections differ by nearly a factor of 2 (relative to the total), which is close to the uncertainty in the experimental normalization of this cross section cited in Ref. 2.

Figure 3 shows the calculated eigenquantum defects in this same energy range, illustrating their extremely smooth dependence on energy. It is striking to visualize how MQDT converts such smooth short-range information into the rapidly energy-dependent cross sections of Fig. 1, in the course of solving Eq. (9). Table III gives the short-range scattering information needed to calculate the Cs^- photodetachment spectrum in the energy range near the $6p$ thresholds. This data is given in the form of a real, symmetric quantum defect matrix μ_{ij} at the two detachment thresholds, defined formally as in Eq. (26) of Ref. 13(a). The eigenquantum defects μ_α to be used in Eqs. (5–8) are simply the eigenvalues of μ_{ij}, while the $U_{i\alpha}$ are its corresponding eigenvectors. The last row shown for each energy in Table III gives dipole matrix elements d_i. From these values, the eigenchannel dipole matrix elements D_α in Eq. (6) connecting the Cs^- ground state to the α-th independent eigenchannel solution are given simply by $D_\alpha = \sum_i d_i U_{i\alpha}$. The quantum-defect matrices give the e-Cs scattering information with respect to the *analytic* base pair of polarization solutions (f_i^0, g_i^0) in all channels except the first two channels in Table I. In these two channels the energy-normalized radial solutions (f_i, g_i) are used instead because they are somewhat smoother functions of energy far above their respective detachment thresholds.

Figure 4 shows partial cross sections for ejection of photoelectrons into each of the seven jj-coupled channels listed in Table I. The partial cross sections for ejection of "fast photoelectrons" are shown in Fig. 4(a), showing that the expected statistical ratio approximately governs the relative cross sections of $6s_{1/2}\epsilon p_{3/2}$ to $6s_{1/2}\epsilon p_{1/2}$, except right at the resonances. Figure 4(b) shows instead the "slow photoelectron" partial cross sections associated with production of excited cesium atoms. These results show that Lee's neglect[5] of d-wave photoelectrons is only a fair approximation, as it is clearly breaking down near the $6p_{3/2}$ threshold. In fact the total cross section at the minimum of the resonance just below the upper threshold is *dominated* by the $6p_{1/2}\epsilon d_{3/2}$ channel, completely ignored by Lee. Lee's semiempirical fit is poorest in this energy range (see, e.g., Fig. 10 of Ref. 2), suggesting that omission of d waves is an important limitation of his semiempirical calculation, in addition to his neglect of the Cs($6p$) polarizability addressed by Refs. 6 and 7. On the other hand the two channels $6p_{3/2}\epsilon d_{3/2}$ and $6p_{3/2}\epsilon d_{5/2}$ are clearly negligible in this energy range as assumed by Lee.

The importance of the $6p_{1/2}\epsilon d_{3/2}$ channel implied by the partial cross section in Fig. 4(b) suggests two immediate experimental consequences. The first derives from Lee's prediction[5] that the slow photoelectrons in Cs^- photodetachment must have an isotropic angular distribution if only s-wave ejection is possible. But as the photon energy goes through the resonance near 15 500 cm^{-1},

TABLE III. Quantum-defect matrices μ_{ij} and reduced dipole matrix elements d_i relevant to Cs^- photodetachment. The channel indices i are in the order shown in Table I.

At the Cs($6p_{1/2}$) threshold						
			μ_{ij}			
0.132 27	0.010 22	−0.078 69	0.028 67	−0.097 42	−0.025 80	−0.000 03
0.010 22	0.103 61	0.105 87	−0.018 80	0.152 67	−0.004 03	−0.031 43
−0.078 69	0.105 87	0.118 67	−0.009 34	−0.045 77	−0.015 57	−0.041 21
0.028 67	−0.018 80	−0.009 34	0.168 12	−0.058 92	0.052 54	−0.031 51
−0.097 42	0.152 67	−0.045 77	−0.058 92	0.088 02	0.030 47	−0.029 09
−0.205 80	−0.004 03	−0.015 57	0.052 54	0.030 47	0.185 61	−0.018 64
−0.000 03	−0.031 43	−0.041 21	−0.031 51	−0.029 09	−0.018 64	0.162 48
			d_i			
0.439 36	−0.698 93	0.028 08	−0.095 37	0.004 02	0.029 00	−0.090 99
At the Cs($6p_{3/2}$) threshold						
			μ_{ij}			
0.133 68	0.008 63	−0.070 81	0.024 70	−0.109 02	−0.024 18	0.000 05
0.008 63	0.104 89	0.110 74	−0.015 52	0.159 86	−0.005 24	−0.029 15
−0.070 81	0.110 74	0.170 37	−0.017 47	−0.060 73	−0.001 71	−0.029 12
0.024 70	−0.015 52	−0.017 47	0.182 68	−0.053 51	0.067 44	−0.044 10
−0.109 02	0.159 86	−0.060 73	−0.053 51	0.143 37	0.023 25	−0.036 87
−0.024 18	−0.005 24	−0.001 71	0.067 44	0.023 25	0.187 94	−0.020 21
0.000 05	−0.029 15	−0.029 12	−0.044 10	−0.036 87	−0.020 21	0.153 11
			d_i			
0.375 64	−0.602 80	0.049 39	−0.104 51	0.057 31	0.034 45	−0.100 00

the dominance of the $6p_{1/2}\epsilon d_{3/2}$ channel implies that the asymmetry parameter for slow photoelectrons will change rapidly from its isotropic value $\beta=0$. In particular it should attain the value $\beta=1$ if the incident photons are linearly polarized at the energy ($\approx 15\,470$ cm^{-1}) in Fig. 4(b) at which the $6p_{1/2}\epsilon s_{1/2}$ partial cross section vanishes.[27]

A second experimental implication of the strong d-wave contribution is a rapid energy dependence of the circular polarization of atomic fluorescence $6p_{1/2}\rightarrow 6s_{1/2}$ observed following photodetachment using circularly polarized incident light. Specifically, as defined in Ref. 28, $O_0 \equiv \langle j_{1z}\rangle / \sqrt{j_1(j_1+1)}$, the "electronic orientation" (ignoring hyperfine depolarization effects) of Cs($6p_{1/2}$) has the "background value" $O_0 = 1/\sqrt{3}$ in the absence of any d-wave contribution. The positive value of this orientation parameter reflects the fact that the $6p_{1/2}$ helicity has the same sense as that of the incident photon, as might be expected from a propensity rule.[29] But as the incident photon energy sweeps through the resonance energy ($\approx 15\,470$ cm^{-1}) at which the $6p_{1/2}\epsilon s_{1/2}$ contribution vanishes, the Cs($6p_{1/2}$) electronic orientation changes sign and reaches the minimum possible theoretical value (for a state having $j_1=\frac{1}{2}$ produced in photodetachment), namely, $O_0 = -1/2\sqrt{3}$. This result is somewhat surprising since the Cs($6p_{1/2}$) state thereby acquires angular momentum in the *opposite sense of rotation* from that of the incident photon helicity. Using Eqs. (17), (36), and (37) of Ref. 28, these values of the *electronic* orientation can be translated into a quantitative prediction for the degree of circular polarization of the atomic fluorescence including hyperfine depolarization.

B. Rb^-

The experimental photodetachment resonances[3,4] of Rb^- near the Rb($5p$) thresholds are reproduced in Fig. 5(a). These bear a remarkable resemblance to the analogous Cs^- resonances. The Rb^- resonance below Rb($5p_{1/2}$) lies clearly closer to the $^2P_{1/2}$ threshold than in Cs^-, and the same observation also holds for the resonance below Rb($5p_{3/2}$). Table I indicates that the polarizability of Cs($6p$) is nearly twice that of Rb($5p$), whereas the atomic np orbitals have nearly the same radius. It appears that the smaller value of the Rb($5p$) polarizability may be at least partially responsible for the diminished attraction of the outermost electron in these resonance states of Rb^-. In any case the calculated photodetachment spectrum for Rb^- in Fig. 5(b) shows roughly the same level of agreement with the experimental spectrum as noted above for Cs^-.

Figure 6(a) shows two different experimental measurements[3,4] of the branching ratio for photoproduction of excited Rb. The fact that the branching ratio above the $5p_{3/2}$ threshold is close to 50% is a reflection of the remarkably strong correlation between the two valence electrons, as this ratio would vanish in the absence of electron correlations. This nearly equal mixing of the lowest two odd-parity channels parallels that observed in $^1P^o$ symmetry of the alkaline-earth atoms,[30,31,10–13] and appears to be a general phenomenon in atoms and negative ions having two valence electrons. Both measurements agree reasonably well with the calculated branching ratio in Fig. 6(b) over the energy range shown, in shape and in magnitude except immediately above the $5p_{1/2}$ threshold.

C. Fr^-

The same basic procedure outlined above has been repeated to obtain a prediction of the photodetachment spectrum of Fr^-. This is motivated by a desire to see the consequences of the much stronger spin-orbit interaction, which in turn enhances the importance of d waves in the photoelectron escape. It is also informative to see to what extent the pattern established for the photodetachment resonances of Rb^- and Cs^- will be continued in Fr^-. It is not obvious in advance that this pattern will remain unchanged, particularly in light of other strong relativistic effects which have been predicted to cause the electron affinity of Ra to be greatly diminished from the trend established for Ca, Sr, and Ba[9(c)].

The nucleus of francium is highly radioactive, its most

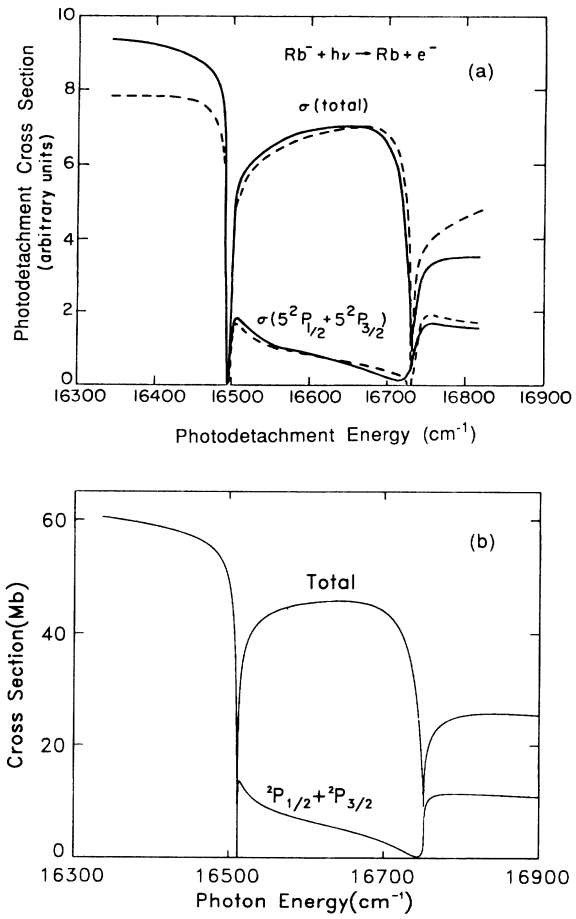

FIG. 5. Total and partial cross sections for photodetachment of Rb^- near the $5p_{1/2}$ and $5p_{3/2}$ thresholds. (a) Experimental relative spectra of Frey *et al.* (Ref. 3) are shown as solid lines, while the dashed curves represent the results of a semiempirical MQDT fit to the data which was conducted by Rouze and Geballe (adapted from Ref. 4). (b) Present calculated spectra.

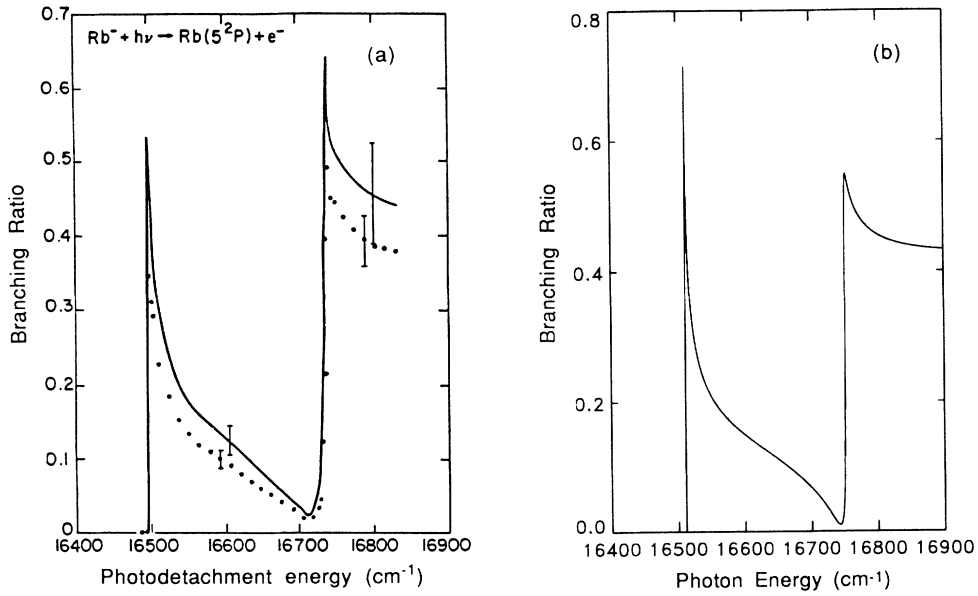

FIG. 6. Branching ratio for production of excited Rb($5p$) states in Rb^- photodetachment. (a) Experiment: solid curve represents data from Frey *et al.* (Ref. 3), while data points are from the measurement of Rouze and Geballe (adapted from Ref. 4). (b) Present calculation.

stable isotope having a half-life of 22 min.[32] Accordingly there is very little spectroscopic data known for the neutral atom, and this experimental information has been acquired relatively recently. For this reason the one-electron potential parameters in Eq. (2), describing the e-Fr^+ interaction, have been modified to reproduce *theoretical levels* of Fr calculated by Dzuba *et al.*[33] adjusted to give the precisely measured[32] spin-orbit splitting $7p_{3/2}-7p_{1/2}$ as accurately as possible.

The resulting channel polarizabilities for the $J^\pi=1^-$ symmetry of Fr^- are shown in Table I. The effective polarizability of the lowest two channels associated with the $7s_{1/2}$ threshold is closer to the static polarizability of Rb than to that of Cs, apparently reflecting the relativistic contraction of inner-shell orbitals. On the other hand the excited-state channel polarizabilities are closer to those for Cs^-. As expected these depend more strongly on the atomic angular momentum quantum number j_1 in Fr^- than in Cs^-, reflecting the greater j_1 dependence of the atomic $n_1l_1j_1$ wave functions and energy levels.

The francium electron affinity predicted by the $J^\pi=0^+$ calculation is 0.514 eV, which is expected to overestimate the binding by approximately 10%, judging from the agreement found for Cs^-. The calculated photodetachment spectrum in Fig. 7 is seen to display the same resonances observed for Rb^- and Cs^-, except for some quantitative differences. One major difference is that the Fr^- autodetaching resonance below the $7p_{1/2}$ threshold is not a pure "window" resonance as in Rb^- and Cs^-, but rather it shows a pronounced asymmetry. As in the lighter negative ions, however, this resonance lies very close to the $p_{1/2}$ threshold; this is more evident in the expanded spectrum shown in Fig. 8(a). Moreover, the resonance below the $7p_{1/2}$ threshold minimizes at a value of approximately 10% of the background, which is $2\frac{1}{2}$ times that calculated for Cs^-. The fine-structure splitting of Fr($7p$) is about 3 times larger than that of Cs($6p$), apparently verifying that the nonzero value of the resonance minimum is correlated with the strength of the spin-orbit interaction. Comparison of Fig. 8(b) with Fig. 4(b) shows that the d- wave contribution to the slow photoelectron partial cross section is larger in Fr^- than in Cs^- near the $p_{3/2}$ threshold by a factor in the range of 3 to 5, correlating also with the greater spin-orbit splitting in Fr.

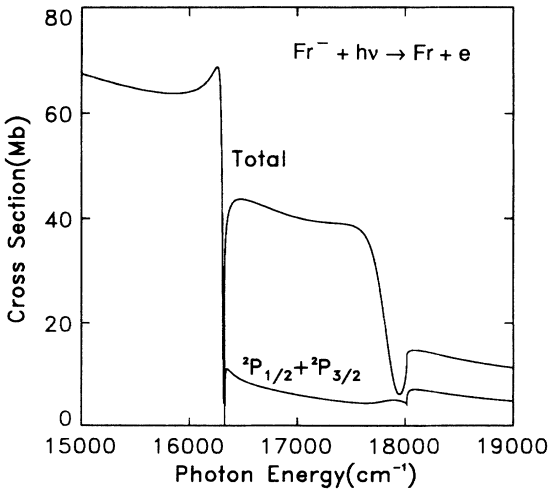

FIG. 7. Predicted cross sections for photodetachment of the Fr^- negative ion near the first excited $7p_{1/2}$ and $7p_{3/2}$ thresholds of Fr.

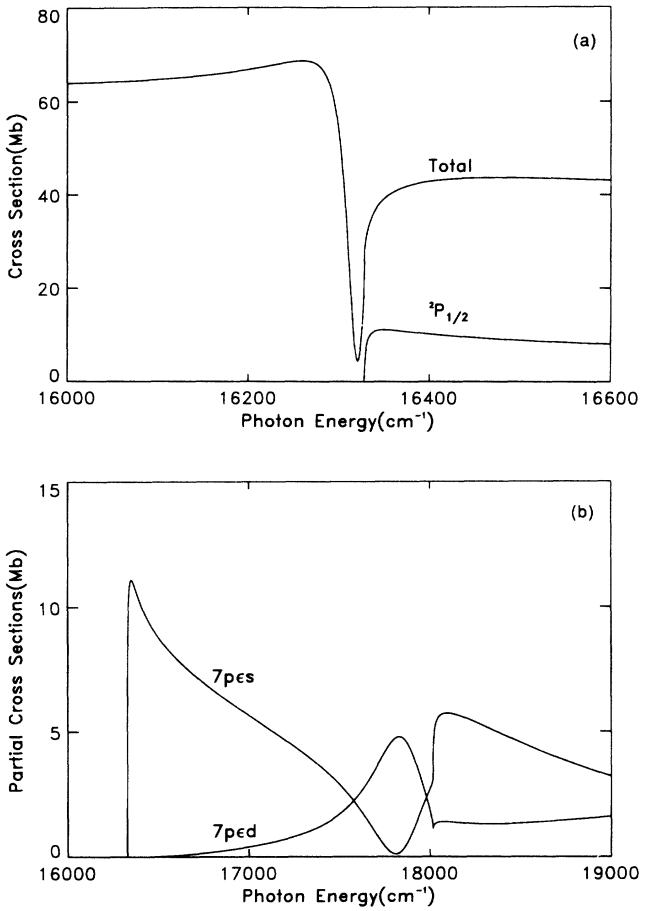

FIG. 8. (a) Expanded view of the total and partial cross sections for Fr^- photodetachment near the $7p_{1/2}$ threshold. (b) Partial cross sections for production of slow photoelectrons in Fr^- photodetachment in either s or d waves, showing greater importance of d waves compared to Cs^-.

IV. CONCLUSIONS

Extensive and detailed studies in recent years[10–14,34] have shown R-matrix and quantum-defect methods to give a highly efficient and accurate description of alkaline-earth atom spectroscopy and dynamics. Very recent work has shown that this description remains accurate even for atoms as heavy as barium.[21,34] The present results verify that these same techniques can be applied with similar confidence to make detailed predictions of photodetachment spectra for the heavy alkali-metal negative ions. The most general conclusion to be drawn is that all of these systems can be treated as "two-electron" systems, provided the "one-electron" spectrum is *constrained* to reproduce the experimental one-electron energy levels. It would be useful to develop eventually a truly *ab initio* method to obtain the one-electron effective potential $V(r)$, as opposed to the present semiempirical method, but the two-electron spectra are not likely to be changed significantly by using a different one-electron potential.

A second major conclusion which is somewhat surprising is that by semiempirically constraining the one-electron energy levels to agree with the experimental alkali-metal levels, some relativistic effects are indirectly included even for atoms as heavy as cesium without their explicit introduction. The relativistic spin-orbit interaction term is included explicitly, of course, and it plays a crucial role in defining the final detailed appearance of the photoabsorption spectrum. But numerous other relativistic effects, such as the relativistic mass effect which is quite large in Cs, are apparently described adequately by the Schrödinger equation as long as experimental energy level information is incorporated into the one-electron potential. The success of this nonrelativistic description may be related to the fact that photoabsorption mainly probes the details of the two-electron wave function beyond one Bohr radius from the nucleus; greater errors should probably be anticipated for short-range observables such as hyperfine structure. Still, this amounts to an economical method for describing perturbative relativistic effects without appealing to the full complexity of methods based on the Dirac equation.

The e-Cs scattering calculations of Scott *et al.*[19] are similar in their use of a semiempirical model potential. The main differences in practice stem from their use of the Wigner-Eisenbud formulation of R-matrix theory as opposed to the present eigenchannel treatment. In addition, Ref. 19 solves the full set of close-coupling equations to obtain the scattering electron wave function outside the R-matrix box, whereas the present treatment of large-r electron motion is based on an MQDT formulation for the polarization potential. The incorporation of additional multipoles by Ref. 19 outside the R-matrix box is likely to be somewhat more accurate than the present MQDT approach, but MQDT is expected to be more efficient for the calculation of rapidly varying resonance features requiring a fine energy mesh. An R-matrix box radius $r_0=30$ a.u. was used for all calculations of this paper, which is much smaller than the value $r_0=40.4$ a.u. used in Ref. 19. A larger box radius was presumably used in Ref. 19 because they consider excitations of the Cs($5d$) levels in addition to the Cs($6p$) states.

A few tests of the r_0 dependence of the calculated photodetachment spectra in this paper have shown it to be generally weak, but somewhat stronger than had been found in previous studies of the neutral alkaline-earth atoms.[10–13,21,34] This residual r_0 dependence deserves some further attention, and is being investigated systematically by Rouze in the context of K^- photodetachment.[35] A more complete treatment of long-range multipole effects within the MQDT formulations is also desirable, and should be straightforward along the lines discussed in Ref. 36.

Finally, the growing evidence for excited Cs^- $^3P^o$ bound levels, which derives from Refs. 16–19 in addition to the present study, warrants some experimental effort. It is difficult to have complete complete confidence in any of the theoretical calculations, in view of the small binding energies predicted, but the agreement between several different methods of calculation is highly suggestive. Moreover, the experimental signature for these levels should be clear if they are formed in a Cs^- beam and photodetached in the vicinity of the $6p$ thresholds.

ACKNOWLEDGMENTS

Extensive discussions with M. Aymar concerning the inclusion of spin-orbit effects in eigenchannel R-matrix calculations played a key role in the completion of this work. Conversations with P. Schulz and W. C. Lineberger, and access to unpublished experimental results of Ref. 25, have been helpful, as have discussions with N. Rouze. The support and hospitality of M. Le Dourneuf, J. M. Launay, and P. G. Burke during a Centre Européen de Calcul Atomique et Moléculaire (CECAM) workshop in Meudon, France are appreciated. I thank S. Watanabe for providing a computer program to calculate quantum-defect parameters and wave functions for a polarization potential. All computations have been carried out on a Digital Equipment Corporation DECstation 3100. This work was supported in part by the National Science Foundation.

[1]T. A. Patterson, H. Hotop, A. Kasdan, D. W. Norcross, and W. C. Lineberger, Phys. Rev. Lett. **32**, 189 (1974).

[2]J. Slater, F. H. Read, S. E. Novick, and W. C. Lineberger, Phys. Rev. A **17**, 201 (1978).

[3]P. Frey, F. Breyer, and H. Hotop, J. Phys. B **111**, L589 (1978); P. Frey, M. Lawen, H. Klar, and H. Hotop, Z. Phys. A **304**, 155 (1982); **306**, 185(E) (1982).

[4]N. Rouze and R. Geballe, Phys. Rev. A **27**, 3071 (1983).

[5]C. M. Lee, Phys. Rev. A **11**, 1692 (1975).

[6]K. T. Taylor and D. W. Norcross, Phys. Rev. A **34**, 3878 (1986).

[7]S. Watanabe and C. H. Greene, Phys. Rev. A **22**, 158 (1980).

[8]M. J. Seaton, Rep. Prog. Phys. **46**, 97 (1983); U. Fano and A. R. P. Rau, *Atomic Collisions and Spectra* (Academic, Orlando, 1986).

[9](a) S. Watanabe, Phys. Rev. A **25**, 2074 (1982); (b) S. Watanabe, J. Phys. B **19**, 1577 (1986); (c) L. Kim and C. H. Greene, J. Phys. B **22**, L175 (1989).

[10]C. H. Greene, in *Fundamental Processes of Atomic Dynamics,* edited by J. Briggs, H. Kleinpoppen, and H. Lutz (Plenum, New York, 1988), p. 105; also C. H. Greene and L. Kim, Phys. Rev. A **38**, 5953 (1988).

[11]P. F. O'Mahony and C. H. Greene, Phys. Rev. A **31**, 250 (1985); P. F. O'Mahony, Phys. Rev. A **32**, 908 (1985).

[12]M. Aymar, E. Luc-Koenig, and S. Watanabe, J. Phys. B **20**, 4325 (1987); M. Aymar, J. Phys. B **20**, 6507 (1987).

[13](a) C. H. Greene and L. Kim, Phys. Rev. A **36**, 2706 (1987); (b) L. Kim and C. H. Greene, Phys. Rev. A **36**, 4272 (1987).

[14]K. Bartschat, M. R. H. Rudge, and P. Scott, J. Phys. B **19**, 2469 (1986).

[15]See, e.g., E. Y. Xu, Y. Zhu, O. P. Mullins, and T. F. Gallagher, Phys. Rev. A **33**, 2401 (1986); *ibid.* **35**, 1138 (1987); V. Lange, U. Eichmann, and W. Sandner, J. Phys. B **22**, L245 (1989); K. Ueda and K. Ito, Phys. Scr. (to be published); U. Griesmann, N. Shen, J. P. Connerade, K. Sommer, and J. Hormes, J. Phys. B **21**, L83 (1988).

[16]C. F. Fischer and D. Chen, J. Mol. Struct. **199**, 61 (1989).

[17]I. I. Fabrikant, Opt. Spektrosk. **53** 223 (1982) [Opt. Spectrosc. (USSR) **53**, 131 (1982)].

[18]J. L. Krause and R. S. Berry, Comments At. Mol. Phys. **18**, 91 (1986).

[19]N. S. Scott, K. Bartschat, P. G. Burke, O. Nagy, and W. B. Eissner, J. Phys. B **17** 3755 (1984).

[20]E. U. Condon and G. H. Shortley, *The Theory of Atomic Spectra* (Cambridge University Press, 1935).

[21]M. Aymar (unpublished), and also Ref. 12.

[22]H. L. Zhou and D. W. Norcross, Phys. Rev. A **40** 5048 (1989).

[23]W. Johnson, D. Kolb, and K.-N. Huang, At. Data Nucl. Data Tables **28**, 333 (1983).

[24]The parameters β_i $\mathcal{G}_l$, and A_l for p and d waves are available upon written request from the author (or via bitnet, CHG @ JILA).

[25]C. H. Greene and Ch. Jungen, Adv. At. Mol. Phys. **21**, 51 (1985).

[26]P. Schulz, R. Mead, and W. C. Lineberger (private communication).

[27]U. Fano and D. Dill, Phys. Rev. A **6**, 185 (1972). See Eq. (15) of this reference, using $j_t=1$, $j_r=1$, $m_r=0$, $l=l'=2$.

[28]C. H. Greene and R. N. Zare, Annu. Rev. Phys. Chem. **33**, 119 (1982).

[29]C. H. Greene, in *Fundamental Processes of Atomic Dynamics,* edited by J. S. Briggs, H. Kleinpoppen and H. O. Lutz (Plenum, New York, 1988), p. 177.

[30]J. J. Wynne and J. A. Armstrong, Comments At. Mol. Phys. **8**, 155 (1979).

[31]C. H. Greene, Phys. Rev. A **23**, 661 (1981).

[32]J. Bauche, H. T. Duong, P. Juncar, S. Liberman, J. Pinard, A. Coc, C. Thibault, F. Touchard, J. Lerme, J. L. Vialle, S. Büttgenbach, A. C. Mueller, A. Pesnelle, and the ISOLDE collaboration, J. Phys. B **19** L593 (1986).

[33]V. A. Dzuba, V. V. Flambaum, and O. P. Sushkov, Phys. Lett. **95A**, 230 (1983).

[34]C. H. Greene and M. Aymar (unpublished).

[35]N. Rouze (unpublished).

[36]C. H. Greene, A. R. P. Rau, and U. Fano, Phys. Rev. A **26**, 2441 (1982).